

Bulk Motion in Global AdS₃ from the Boundary Energy-Density Perspective

Shiki Yoshikawa

Department of Physics, Kyoto University, Kyoto 606-8502, Japan

yoshikawa.shiki@gauge.scphys.kyoto-u.ac.jp

May 29, 2026

Abstract

We study how bulk propagation in global AdS₃ is encoded in boundary energy densities of the dual CFT₂ on the cylinder. A key feature of the global geometry, which is absent in the Poincaré-patch description, is that a null excitation emitted from the boundary reaches the antipodal boundary point after $\Delta\tau = \pi$ and returns to the original boundary point after $\Delta\tau = 2\pi$. We show that this periodic boundary-to-boundary propagation is reflected in the CFT energy density as chiral peaks that meet at the antipodal point and reappear after one global period. For a wave-packet state, the leading energy density consists of two chiral peaks moving along the boundary light-cone directions; their relative weights encode the impact parameter of the corresponding bulk null ray. For a state constructed from an operator of large conformal dimension with a Euclidean time regulator (LCD state), the exact cylinder stress tensor gives two periodic chiral pulses moving along the boundary light-cone directions. These pulses reach the antipodal point and return to the original point at the same global times as the radial null geodesic in the bulk. Thus the boundary energy density captures the boundary-to-boundary propagation and periodicity of localized bulk excitations in global AdS₃.

Contents

1	Introduction and summary	3
2	Null geodesics and wave-packet states	5
2.1	Null geodesics in global AdS_3	5
2.2	Wave-packet state on the boundary cylinder	7
2.3	Exact cylinder correlators	8
2.4	Energy density for wave-packet state	9
2.5	Small-width approximation	10
2.6	Contour integral and dominant pole contributions	12
2.7	Periodization on the boundary cylinder	16
3	LCD state and radial null propagation	17
3.1	Exact cylinder stress tensor	19
3.2	Lorentzian energy density and comparison with the bulk profile	20
4	Discussion	21
A	Bulk wave packet from global Klein–Gordon modes	24
A.1	Global modes and the wave-packet state	24
A.2	Bulk profile and stationary phase	26
A.3	Null geodesic from the stationary-phase conditions	28
B	Bulk interpretation of the LCD state	31

1 Introduction and summary

One of the basic questions in holography is how bulk propagation is encoded in the dual boundary theory in AdS/CFT [1–3]. More generally, this question is part of the broader problem of bulk reconstruction and the emergence of local bulk physics in AdS/CFT [4–7]. In this paper we focus on a simple aspect of this problem: how boundary-to-boundary bulk propagation in global AdS₃ is reflected in boundary energy densities of the dual CFT₂ on the cylinder.

The global patch is particularly useful for this purpose. A null ray emitted from the boundary reaches the antipodal boundary point after $\Delta\tau = \pi$ and returns to the original boundary point after $\Delta\tau = 2\pi$. This boundary-to-boundary propagation is not visible in the same way in a Poincaré-patch description. The natural question is therefore how this global propagation appears in boundary observables on the cylinder. This is closely related to the appearance of bulk-cone singularities in Lorentzian CFT correlators, which reflect bulk null propagation [8,9].

In this paper we focus on the boundary energy density as a simple observable that can be computed explicitly in the states we consider. We will not assume that the energy density literally draws the bulk trajectory. Rather, we ask whether it reflects the arrival of the bulk null ray at the antipodal boundary point, its subsequent return to the original boundary point, and the associated periodicity of global AdS propagation.¹

Wave packets have played an important role in studies of bulk locality and scattering in AdS/CFT [12,13]. A useful starting point for the present problem is the wave-packet construction of [14], where the CFT energy density associated with a bulk wave packet in AdS₃/CFT₂ was shown to be localized in two light-like peaks. Since that analysis was carried out in a Poincaré patch, it does not directly display the periodic boundary-to-boundary propagation of global AdS. We therefore reformulate the wave-packet analysis on the global cylinder and study how the local light-like peaks appear as periodic chiral peaks in the boundary energy density.

We also study a second class of states constructed from a local scalar primary operator of large conformal dimension, with a Euclidean time regulator. We refer to this state as the large-conformal-dimension operator state (LCD state). This construction is related to earlier holographic local-quench setups, where local CFT excitations were used to probe localized bulk dynamics [15,16], and more directly to the localized global-AdS states constructed in [17]. More generally, Euclidean sources provide a way to prepare Lorentzian semiclassical bulk states in holographic CFTs [18]. This example is useful for our purpose because the boundary stress tensor can be computed exactly. The resulting energy density consists of two chiral pulses moving along the boundary light-cone directions. We compare this behavior with the

¹We do not assume that the bulk motion must be reproduced as a literal local propagation on the boundary [10]. The point is rather that the boundary-to-boundary propagation and periodicity implied by bulk motion should be encoded consistently in boundary observables. See also [11] for related discussions on bulk locality and bulk local states.

corresponding bulk profile and show that the boundary pulses reach the antipodal point and return to the original point at the same global times as the radial null geodesic in global AdS. Thus this state provides another example in which the periodic boundary-to-boundary propagation of a localized bulk excitation is visible in the boundary energy density.

In Section 2, we first review null geodesics in global AdS₃ and then analyze the boundary wave-packet state. We derive the energy density from exact cylinder correlators. In the small-width regime, the leading contribution comes from local neighborhoods of the nearest pole. The resulting energy density consists of two periodic chiral peaks moving along the boundary light-cone directions. Here “chiral” refers to the holomorphic and anti-holomorphic components of the two-dimensional CFT stress tensor. In Lorentzian signature these components propagate along the boundary light-cone directions

$$u = \frac{t}{L} + \theta, \quad v = \frac{t}{L} - \theta.$$

Their relative weights encode the impact parameter of the corresponding bulk null ray, while their propagation on the cylinder reproduces the arrival at the antipodal boundary point and the subsequent return to the original boundary point.

In Section 3, we analyze the LCD state. We compute the exact cylinder stress tensor and find two periodic chiral pulses in the boundary energy density. We then compare this result with the bulk profile in global AdS, whose behavior is governed by a radial null geodesic. The boundary pulses reach the antipodal point and return to the original point at the same global times as this radial null propagation.

In Section 4, we summarize the comparison between the two examples and discuss possible extensions. In particular, we comment on how the periodic structure found in pure global AdS may be modified in black-hole backgrounds, and on which features of the result are special to AdS₃/CFT₂.

The appendices provide the bulk interpretation of the two states used in the main text. In Appendix A, we analyze the bulk behavior of the wave-packet state using global Klein–Gordon modes. In Appendix B, we study the bulk profile of the LCD state using global AdS modes.

The main conclusion of this paper is that the global cylinder description makes the boundary-to-boundary propagation and periodicity of localized bulk excitations visible in boundary energy densities. For the wave-packet state, the leading energy density is obtained from the exact cylinder correlators. For the LCD state, the exact boundary stress tensor shows the same arrival at the antipodal boundary point and subsequent return to the original point as the radial null geodesic. Together, these examples show that boundary energy densities on the cylinder encode the boundary-to-boundary propagation and periodicity of localized bulk excitations in global AdS₃.

2 Null geodesics and wave-packet states

2.1 Null geodesics in global AdS₃

In this subsection we use the dimensionless global time τ . The corresponding dimensionful boundary time used in the CFT calculation below is $t = L\tau$. We use the global AdS₃ metric

$$ds^2 = \frac{L^2}{\cos^2 \rho} (-d\tau^2 + d\rho^2 + \sin^2 \rho d\theta^2), \quad 0 \leq \rho < \frac{\pi}{2}, \quad \theta \sim \theta + 2\pi. \quad (2.1)$$

The conformal boundary is the cylinder $\mathbb{R} \times S^1$ with metric

$$ds_{\partial}^2 \sim -d\tau^2 + d\theta^2. \quad (2.2)$$

We first consider general null geodesics. Because τ and θ are Killing coordinates, the motion has two conserved quantities,

$$E := -p_{\tau} = \frac{L^2}{\cos^2 \rho} \dot{\tau}, \quad J := p_{\theta} = \frac{L^2 \sin^2 \rho}{\cos^2 \rho} \dot{\theta} = L^2 \tan^2 \rho \dot{\theta}, \quad (2.3)$$

where the dot denotes differentiation with respect to an affine parameter. It is convenient to introduce the impact parameter²

$$b := \frac{J}{E}. \quad (2.4)$$

The null condition $ds^2 = 0$ gives

$$-\dot{\tau}^2 + \dot{\rho}^2 + \sin^2 \rho \dot{\theta}^2 = 0 \quad (2.5)$$

after removing the overall conformal factor in (2.1). Using (2.3), we obtain

$$\dot{\rho}^2 = \frac{\cos^4 \rho}{L^4} \left(E^2 - \frac{J^2}{\sin^2 \rho} \right). \quad (2.6)$$

Dividing by $\dot{\tau}^2$, this becomes

$$\left(\frac{d\rho}{d\tau} \right)^2 = 1 - \frac{b^2}{\sin^2 \rho}. \quad (2.7)$$

Hence the turning point $\rho = \rho_*$ is determined by

$$\sin \rho_* = |b|, \quad (2.8)$$

²Strictly speaking, in global AdS this quantity is simply the ratio of the conserved angular momentum and energy along the geodesic. We nevertheless refer to it as an impact parameter by analogy with the standard terminology in geodesic motion; see also [19] for a related discussion.

so a boundary-to-boundary null geodesic exists for $0 \leq |b| \leq 1$. The case $|b| = 1$ is the limiting boundary null curve.

The angular motion is obtained from

$$\frac{d\theta}{d\tau} = \frac{\dot{\theta}}{\dot{\tau}} = \frac{J}{E \sin^2 \rho} = \frac{b}{\sin^2 \rho}. \quad (2.9)$$

Choosing $\tau = 0$ at a boundary point and following the geodesic into the bulk, one finds from (2.7)

$$\cos \rho(\tau) = \sqrt{1 - b^2} \sin \tau, \quad 0 \leq \tau \leq \pi. \quad (2.10)$$

At $\tau = 0$ and $\tau = \pi$ one has $\rho = \pi/2$, while at $\tau = \pi/2$ one reaches the turning point $\rho = \rho_*$. Using the angular equation together with (2.10), we obtain

$$\frac{d\theta}{d\tau} = \frac{b}{1 - (1 - b^2) \sin^2 \tau} = \frac{b}{\cos^2 \tau + b^2 \sin^2 \tau}. \quad (2.11)$$

For $b > 0$, this integrates to

$$\theta(\tau) = \theta_0 + \begin{cases} \arctan(b \tan \tau), & 0 \leq \tau \leq \pi/2, \\ \pi + \arctan(b \tan \tau), & \pi/2 \leq \tau \leq \pi. \end{cases} \quad (2.12)$$

For $b < 0$ the angular orientation is reversed. In either case, modulo 2π ,

$$\theta(0) = \theta_0, \quad \theta(\pi) = \theta_0 + \pi. \quad (2.13)$$

Thus the boundary endpoints are antipodal independently of b , although the radial depth of the geodesic depends on b .

Therefore the boundary-to-boundary data for null geodesics are

$$\Delta\tau_{\text{bulk}}^{\text{null}} = \pi, \quad \Delta\theta_{\text{bulk}}^{\text{null}} = \pi. \quad (2.14)$$

In terms of the dimensionful boundary time $t = L\tau$, this is

$$\Delta t_{\text{bulk}}^{\text{null}} = \pi L. \quad (2.15)$$

After one full global period the ray returns to the original boundary point,

$$\Delta\tau_{\text{period}}^{\text{null}} = 2\pi, \quad \text{or equivalently} \quad \Delta t_{\text{period}}^{\text{null}} = 2\pi L. \quad (2.16)$$

This sequence of boundary arrivals is what we will compare with the periodic chiral peaks in the boundary wave-packet energy density. This behavior is illustrated in Fig. 1.

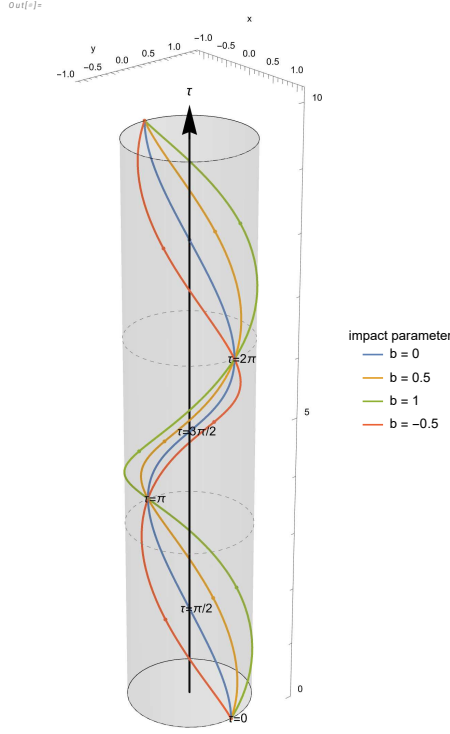


Figure 1: Bulk null geodesics in global AdS_3 shown in a compactified spatial disk times the global time direction, for several values of the impact parameter b . The geodesics start from the boundary at $\tau = 0$, reach a turning point at $\tau = \pi/2$, arrive at the antipodal boundary point at $\tau = \pi$, and return to the original boundary point at $\tau = 2\pi$. Different values of b change the depth of the trajectory in the bulk, while the boundary-to-boundary data $\Delta\tau = \pi$ and $\Delta\theta = \pi$ are unchanged. The curve with $|b| = 1$ should be understood as the limiting boundary null curve.

2.2 Wave-packet state on the boundary cylinder

We now switch to the dimensionful boundary time

$$t = L\tau. \quad (2.17)$$

The boundary cylinder is therefore described by

$$(t, \theta) \in \mathbb{R} \times [-\pi, \pi), \quad \theta \sim \theta + 2\pi, \quad (2.18)$$

with boundary metric proportional to $-dt^2 + L^2 d\theta^2$. We consider a scalar primary operator \mathcal{O} of dimension Δ , so that

$$h = \bar{h} = \frac{\Delta}{2}. \quad (2.19)$$

We define the smeared state with central frequency ω and central angular momentum m_0 by

$$|\omega, m_0\rangle := \int_{-\infty}^{\infty} dt \int_{-\pi}^{\pi} d\theta f_{\omega, m_0}(t, \theta) \mathcal{O}(t, \theta) |0\rangle, \quad (2.20)$$

with

$$f_{\omega, m_0}(t, \theta) := \exp \left[-\frac{t^2 + 4L^2 \tan^2(\theta/2)}{2a^2} - i\omega t + im_0\theta \right]. \quad (2.21)$$

In the small-width regime, the angular part of the source is a Gaussian smearing localized near $\theta = 0$, since

$$2L \tan \frac{\theta}{2} \simeq L\theta.$$

This construction is motivated by the wave-packet state studied in [14]. The main difference is that here the smearing is placed on the global boundary cylinder. In this paper we work in the small-width and high-frequency wave-packet regime

$$a \ll L, \quad \frac{(\omega L - m_0)a}{L} \gg 1, \quad \frac{(\omega L + m_0)a}{L} \gg 1, \quad \omega L > |m_0|. \quad (2.22)$$

Equivalently, in terms of the light-cone momenta introduced below,

$$p_u = \omega L - m_0, \quad p_v = \omega L + m_0, \quad (2.23)$$

this regime is

$$a \ll L, \quad \frac{p_u a}{L} \gg 1, \quad \frac{p_v a}{L} \gg 1, \quad p_u, p_v > 0. \quad (2.24)$$

The condition $a \ll L$ means that the wave packet is localized on a scale much smaller than the AdS radius. The additional conditions $p_u a/L \gg 1$ and $p_v a/L \gg 1$ ensure that the resulting bulk wave packet is sharply peaked around the central energy ω and angular momentum m_0 , with the direction of angular motion fixed by the sign of m_0 . In Appendix A, we make this bulk interpretation explicit using global normal-mode expansion. The smearing prepares a bulk one-particle wave packet sharply peaked around $\Omega_0 = \omega L$ and $m = m_0$, and the stationary-phase conditions of the bulk profile reproduce the null geodesic equations in global AdS₃.

2.3 Exact cylinder correlators

To formulate the wave-packet analysis directly on the global cylinder, we use the exact cylinder correlators. In the small-width regime $a \ll L$, the smearing integrals are dominated by local neighborhoods of the relevant light-cone poles, where the cylinder correlators reduce to the same local form used in the plane analysis of [14]. Let

$$w = t_E + iL\theta, \quad \bar{w} = t_E - iL\theta \quad (2.25)$$

be Euclidean cylinder coordinates, where t_E has the dimension of length. The Euclidean two-point function is

$$\langle \mathcal{O}(w_1, \bar{w}_1) \mathcal{O}(w_2, \bar{w}_2) \rangle_E = C_{\mathcal{O}} \left(\frac{1}{2L \sinh \frac{w_{12}}{2L}} \right)^\Delta \left(\frac{1}{2L \sinh \frac{\bar{w}_{12}}{2L}} \right)^\Delta. \quad (2.26)$$

After analytic continuation $t_E \rightarrow it$, we define

$$u_{ij} := \frac{t_i - t_j + L(\theta_i - \theta_j) - i\epsilon_{ij}}{L}, \quad v_{ij} := \frac{t_i - t_j - L(\theta_i - \theta_j) - i\epsilon_{ij}}{L}, \quad \epsilon_{ij} := \epsilon_i - \epsilon_j, \quad (2.27)$$

with $\epsilon_1 > \epsilon_2 > \epsilon_3 > 0$. The $i\epsilon$ prescription fixes the ordering of the operators; we follow the standard prescription reviewed in [20]. Then

$$\langle \mathcal{O}(t_1, \theta_1) \mathcal{O}(t_2, \theta_2) \rangle = C_{\mathcal{O}} \left(\frac{1}{2Li \sin(u_{12}/2)} \right)^\Delta \left(\frac{1}{2Li \sin(v_{12}/2)} \right)^\Delta. \quad (2.28)$$

Using the plane-to-cylinder map $z = e^{w/L}$, the stress-tensor transformation law, and the conformal Ward identity, one finds

$$\langle \mathcal{O}_1 T_2 \mathcal{O}_3 \rangle = F_u(1, 2, 3) \langle \mathcal{O}_1 \mathcal{O}_3 \rangle, \quad (2.29)$$

where

$$F_u(1, 2, 3) = -\frac{\Delta}{8L^2} \left(\frac{\sin(u_{13}/2)}{\sin(u_{12}/2) \sin(u_{23}/2)} \right)^2 - \frac{c}{24L^2}. \quad (2.30)$$

The corresponding expression for the anti-holomorphic stress tensor is obtained by replacing u with v . We denote it by $F_v(1, 2, 3)$, so that

$$\langle \mathcal{O}_1 \bar{T}_2 \mathcal{O}_3 \rangle = F_v(1, 2, 3) \langle \mathcal{O}_1 \mathcal{O}_3 \rangle. \quad (2.31)$$

The exact pole structure on the cylinder is manifest:

$$u_{12} = 2\pi n_1, \quad u_{23} = 2\pi n_3, \quad n_1, n_3 \in \mathbb{Z}, \quad (2.32)$$

and similarly in the v sector. The role of the image labels will be explained below.

2.4 Energy density for wave-packet state

The norm of the wave-packet state is

$$N_0 := \langle \omega, m_0 | \omega, m_0 \rangle = \int dt_1 d\theta_1 dt_3 d\theta_3 f_{\omega, m_0}(t_1, \theta_1)^* f_{\omega, m_0}(t_3, \theta_3) \langle \mathcal{O}_1 \mathcal{O}_3 \rangle. \quad (2.33)$$

The holomorphic numerator is

$$N_T(t_2, \theta_2) := \int dt_1 d\theta_1 dt_3 d\theta_3 f_{\omega, m_0}(t_1, \theta_1)^* f_{\omega, m_0}(t_3, \theta_3) \langle \mathcal{O}_1 T_2 \mathcal{O}_3 \rangle, \quad (2.34)$$

and similarly for $N_{\bar{T}}$.

With our convention for the cylinder stress tensor,

$$T_{tt}^{\text{cyl}} = T + \bar{T}. \quad (2.35)$$

We define the boundary energy density by subtracting the vacuum contribution,

$$\mathcal{E}(t_2, \theta_2) := \frac{1}{2\pi} \left[\langle T_{tt}(t_2, \theta_2) \rangle_{\omega, m_0} - \langle T_{tt} \rangle_0 \right] = \frac{1}{2\pi} \left[\frac{N_T(t_2, \theta_2) + N_{\bar{T}}(t_2, \theta_2)}{N_0} + \frac{c}{12L^2} \right]. \quad (2.36)$$

The quantity \mathcal{E} includes the factor $1/(2\pi)$. With the dimensionful boundary time convention used here, the physical energy is

$$E_{\text{CFT}}^{\text{phys}} = L \int_{-\pi}^{\pi} d\theta \mathcal{E}(t, \theta). \quad (2.37)$$

Equivalently, the dimensionless cylinder energy is

$$\Omega_{\text{CFT}} = L E_{\text{CFT}}^{\text{phys}}. \quad (2.38)$$

2.5 Small-width approximation

For $a \ll L$, the smearing integrals are dominated by small neighborhoods of the relevant light-cone poles on the cylinder. In these neighborhoods, the cylinder correlators reduce to the same local functional form as in the plane analysis of [14].

We introduce the pointwise light-cone variables

$$u \equiv \frac{t + L\theta}{L}, \quad v \equiv \frac{t - L\theta}{L}, \quad (2.39)$$

so that

$$t = \frac{L}{2}(u + v), \quad \theta = \frac{u - v}{2}, \quad dt d\theta = \frac{L}{2} du dv. \quad (2.40)$$

For $a \ll L$, the smearing localizes the integral near $\theta = 0$, and

$$4L^2 \tan^2 \left(\frac{\theta}{2} \right) \simeq L^2 \theta^2. \quad (2.41)$$

Hence

$$-\frac{t^2}{2a^2} - \frac{L^2\theta^2}{2a^2} = -\frac{L^2}{4a^2}(u^2 + v^2), \quad (2.42)$$

while the phase factor in $f_{\omega, m_0}(t_1, \theta_1)^* f_{\omega, m_0}(t_3, \theta_3)$ becomes

$$i\omega t - im_0\theta = \frac{i}{2}p_u u + \frac{i}{2}p_v v, \quad (2.43)$$

where

$$p_u := \omega L - m_0, \quad p_v := \omega L + m_0. \quad (2.44)$$

The condition $\omega L > |m_0|$ is equivalent to $p_u, p_v > 0$.

Before taking the local approximation, let us clarify the relation between the local computation below and the exact cylinder contour integral. In the exact cylinder correlator, the observation-point singularities form an infinite periodic images. For $a \ll L$, the Gaussian smearing makes the neighborhoods of different images well separated. The local calculation below computes the residue near the nearest image, and the periodic result is obtained by summing the corresponding leading pole contributions from the periodic images.

We now compute explicitly the local contribution from the image poles which dominates near $u_2 = 0$. This is the nearest image, $n_1 = n_3 = 0$. Near the corresponding observation-point singularities, $u_{12} \simeq 0$ and $u_{23} \simeq 0$, the first term in (2.30) reduces to

$$-\frac{\Delta}{8L^2} \left(\frac{\sin(u_{13}/2)}{\sin(u_{12}/2) \sin(u_{23}/2)} \right)^2 \simeq -\frac{\Delta}{2L^2} \left(\frac{u_{13}}{u_{12}u_{23}} \right)^2. \quad (2.45)$$

This gives the local contribution to the peak near $u_2 = 0$.

Let us specify which image poles contributes at leading order near each peak. The exact cylinder correlator has image poles

$$u_{12} = 2\pi n_1, \quad u_{23} = 2\pi n_3, \quad n_1, n_3 \in \mathbb{Z}. \quad (2.46)$$

For a peak centered at $u_2 \simeq 2\pi k$, these pole conditions imply

$$u_1 \simeq u_2 + 2\pi n_1, \quad u_3 \simeq u_2 - 2\pi n_3. \quad (2.47)$$

Since the smearing localizes the source insertions near $u_1 \simeq 0$ and $u_3 \simeq 0$, the leading pole pair near this peak is

$$n_1 = -k, \quad n_3 = k. \quad (2.48)$$

All other pole pairs force at least one of u_1 or u_3 to be displaced from the smearing center by an amount of order 2π , and are therefore exponentially suppressed as $\exp[-\text{const. } L^2/a^2]$ for $a \ll L$. Thus the calculation below is the local residue calculation for the nearest peak; the periodic copies are obtained by shifting to the corresponding leading pole pair and summing

over k .

The local expression for the holomorphic numerator is

$$\begin{aligned}
N_T(u_2, v_2) &\simeq \left(\frac{L}{2}\right)^2 \tilde{C}_O \int du_1 dv_1 du_3 dv_3 \exp \left[-\frac{L^2}{4a^2} (u_1^2 + v_1^2 + u_3^2 + v_3^2) \right] \\
&\times \exp \left[\frac{i}{2} (p_u u_1 + p_v v_1 - p_u u_3 - p_v v_3) \right] \\
&\times \left[-\frac{\Delta}{2L^2} \left(\frac{u_{13}}{u_{12}u_{23}} \right)^2 - \frac{c}{24L^2} \right] \frac{1}{(u_{13})^\Delta (v_{13})^\Delta}. \tag{2.49}
\end{aligned}$$

Here \tilde{C}_O includes the constant factors from the local limit of the two-point function, and

$$u_{ij} = u_i - u_j - \frac{i\epsilon_{ij}}{L}, \quad v_{ij} = v_i - v_j - \frac{i\epsilon_{ij}}{L}, \quad \epsilon_{ij} := \epsilon_i - \epsilon_j, \quad \epsilon_1 > \epsilon_2 > \epsilon_3 > 0. \tag{2.50}$$

The first term in the square brackets contains the two poles in the nearest image, $u_1 = u_2$ and $u_3 = u_2$, and gives the leading local light-cone peak near $u_2 = 0$. The corresponding leading pole pairs near $u_2 = 2\pi k$ give the periodic copies of this peak on the cylinder.

2.6 Contour integral and dominant pole contributions

We now keep the intermediate residue analysis, since it explains which poles of the cylinder correlator produce the leading energy-density peaks. We follow the contour argument of [10, 14], adapted to the present notation. In this subsection the explicit residue calculation is written for $\Delta \in \mathbb{Z}_{>0}$ for simplicity. For non-integer Δ , the same contour deformation crosses branch cuts rather than isolated poles. In that case, one can deform the contour to wrap around the relevant branch cuts, as in [14], and the leading contribution is obtained from the discontinuity across the cuts. Thus the residue language used below should be understood as a convenient shorthand for the corresponding branch-cut contribution. The final small-width expression is not restricted to integer operator dimensions.

We first extract the first term in the square brackets of (2.49), which contains double poles. Up to the overall prefactor

$$\left(\frac{L}{2}\right)^2 \tilde{C}_O \left(-\frac{\Delta}{2L^2}\right), \tag{2.51}$$

we define

$$\begin{aligned}
A &:= \int du_1 dv_1 du_3 dv_3 \exp \left[-\frac{L^2}{4a^2} (u_1^2 + v_1^2 + u_3^2 + v_3^2) + \frac{i}{2} (p_u u_1 + p_v v_1 - p_u u_3 - p_v v_3) \right] \\
&\times \frac{u_{13}^2}{u_{12}^2 u_{23}^2 (u_{13})^\Delta (v_{13})^\Delta}. \tag{2.52}
\end{aligned}$$

Completing the square gives

$$A = e^{-\frac{a^2}{2L^2}(p_u^2+p_v^2)} \int du_1 dv_1 du_3 dv_3 \exp \left[-\frac{L^2}{4a^2} \left(u_1 - \frac{ip_u a^2}{L^2} \right)^2 - \frac{L^2}{4a^2} \left(v_1 - \frac{ip_v a^2}{L^2} \right)^2 \right] \\ \times \exp \left[-\frac{L^2}{4a^2} \left(u_3 + \frac{ip_u a^2}{L^2} \right)^2 - \frac{L^2}{4a^2} \left(v_3 + \frac{ip_v a^2}{L^2} \right)^2 \right] \frac{u_{13}^2}{u_{12}^2 u_{23}^2 (u_{13})^\Delta (v_{13})^\Delta}. \quad (2.53)$$

The shifts are written in terms of the dimensionless variables u, v .

The v -dependent part is

$$I_v := e^{-\frac{a^2}{2L^2}p_v^2} \int_{\mathbb{R}} dv_1 \int_{\mathbb{R}} dv_3 \exp \left[-\frac{L^2}{4a^2} \left(v_1 - \frac{ip_v a^2}{L^2} \right)^2 - \frac{L^2}{4a^2} \left(v_3 + \frac{ip_v a^2}{L^2} \right)^2 \right] \frac{1}{(v_1 - v_3 - \frac{i\epsilon_{13}}{L})^\Delta}. \quad (2.54)$$

Here $\epsilon_{13} = \epsilon_1 - \epsilon_3 > 0$. Thus, for fixed real v_3 , the singularity in the v_1 plane is located at

$$v_1 = v_3 + \frac{i\epsilon_{13}}{L}, \quad (2.55)$$

slightly above the original v_1 -integration contour.

For integer Δ , we use

$$\frac{1}{(v_1 - v_3 - \frac{i\epsilon_{13}}{L})^\Delta} = \frac{(-1)^{\Delta-1}}{\Gamma(\Delta)} \partial_{v_1}^{\Delta-1} \frac{1}{v_1 - v_3 - \frac{i\epsilon_{13}}{L}}. \quad (2.56)$$

After integrating by parts $\Delta - 1$ times, this gives

$$I_v = e^{-\frac{a^2}{2L^2}p_v^2} \frac{1}{\Gamma(\Delta)} \int_{\mathbb{R}} dv_1 \int_{\mathbb{R}} dv_3 \frac{1}{v_1 - v_3 - \frac{i\epsilon_{13}}{L}} \\ \times \partial_{v_1}^{\Delta-1} \exp \left[-\frac{L^2}{4a^2} \left(v_1 - \frac{ip_v a^2}{L^2} \right)^2 - \frac{L^2}{4a^2} \left(v_3 + \frac{ip_v a^2}{L^2} \right)^2 \right]. \quad (2.57)$$

For $p_v > 0$, the saddle of the v_1 Gaussian is at

$$v_1 = \frac{ip_v a^2}{L^2}. \quad (2.58)$$

We deform the v_1 -integration contour upward to

$$v_1 \in \mathbb{R} + \frac{ip_v a^2}{L^2}. \quad (2.59)$$

Because of the $i\epsilon$ prescription, the pole $v_1 = v_3 + i\epsilon_{13}/L$ lies between the original contour

and the deformed one. Therefore the deformation crosses this pole. The integral over the deformed contour is exponentially suppressed in the wave-packet regime $p_v a/L \gg 1$, and the leading contribution comes from the crossed pole.

Taking the residue, we obtain

$$I_v \simeq \frac{2\pi i}{\Gamma(\Delta)} e^{-\frac{a^2}{2L^2} p_v^2} \int_{\mathbb{R}} dv_3 \partial_{v_1}^{\Delta-1} \exp \left[-\frac{L^2}{4a^2} \left(v_1 - \frac{ip_v a^2}{L^2} \right)^2 - \frac{L^2}{4a^2} \left(v_3 + \frac{ip_v a^2}{L^2} \right)^2 \right] \Big|_{v_1=v_3}. \quad (2.60)$$

In the regime $p_v a/L \gg 1$, the derivative is dominated by

$$\partial_{v_1}^{\Delta-1} \exp \left[-\frac{L^2}{4a^2} \left(v_1 - \frac{ip_v a^2}{L^2} \right)^2 \right] \Big|_{v_1=v_3} \simeq \left(\frac{ip_v}{2} \right)^{\Delta-1} \exp \left[-\frac{L^2}{4a^2} \left(v_3 - \frac{ip_v a^2}{L^2} \right)^2 \right]. \quad (2.61)$$

The exponential factors combine as

$$e^{-\frac{a^2}{2L^2} p_v^2} \exp \left[-\frac{L^2}{4a^2} \left(v_3 - \frac{ip_v a^2}{L^2} \right)^2 - \frac{L^2}{4a^2} \left(v_3 + \frac{ip_v a^2}{L^2} \right)^2 \right] = \exp \left[-\frac{L^2 v_3^2}{2a^2} \right]. \quad (2.62)$$

Thus

$$I_v \simeq (2\pi)^{3/2} \frac{a}{L} \frac{i^\Delta}{\Gamma(\Delta)} \left(\frac{p_v}{2} \right)^{\Delta-1}, \quad (2.63)$$

up to corrections suppressed in the large $p_v a/L$ expansion.

Next we consider the u -dependent part,

$$I_u := e^{-\frac{a^2}{2L^2} p_u^2} \int du_1 du_3 \exp \left[-\frac{L^2}{4a^2} \left(u_1 - \frac{ip_u a^2}{L^2} \right)^2 - \frac{L^2}{4a^2} \left(u_3 + \frac{ip_u a^2}{L^2} \right)^2 \right] \frac{u_{13}^2}{u_{12}^2 u_{23}^2 (u_{13})^\Delta}. \quad (2.64)$$

Here

$$u_{12} = u_1 - u_2 - \frac{i\epsilon_{12}}{L}, \quad u_{23} = u_2 - u_3 - \frac{i\epsilon_{23}}{L}, \quad \epsilon_{12}, \epsilon_{23} > 0. \quad (2.65)$$

Thus the pole $u_{12} = 0$ lies slightly above the original u_1 contour, while the pole $u_{23} = 0$ lies slightly below the original u_3 contour. For $p_u > 0$, the saddle of the u_1 Gaussian lies at $u_1 = ip_u a^2/L^2$. We deform the u_1 contour upward to this saddle. Because of the $i\epsilon$ prescription, this deformation crosses the pole $u_{12} = 0$. The integral over the deformed contour is exponentially suppressed in the wave-packet regime $p_u a/L \gg 1$, and the leading contribution comes from this crossed pole.

Taking the double-pole residue at $u_1 = u_2$, we obtain

$$I_u \simeq 2\pi i e^{-\frac{a^2}{2L^2}p_u^2} \exp \left[-\frac{L^2}{4a^2} \left(u_2 - \frac{ip_u a^2}{L^2} \right)^2 \right] \int du_3 \exp \left[-\frac{L^2}{4a^2} \left(u_3 + \frac{ip_u a^2}{L^2} \right)^2 \right] \\ \times \frac{1}{(u_{23})^\Delta} \left[\frac{ip_u}{2} - \frac{L^2 u_2}{2a^2} - (\Delta - 2) \frac{1}{u_{23}} \right]. \quad (2.66)$$

The term proportional to u_2 is suppressed by $(p_u a/L)^{-1}$ near the leading peak and will be omitted below.

We next deform the u_3 contour downward to the saddle $u_3 = -ip_u a^2/L^2$. Because of the $i\epsilon$ prescription, this deformation crosses the pole $u_{23} = 0$. The integral over the deformed contour is again exponentially suppressed, so the leading contribution comes from the crossed pole at $u_3 = u_2$. Evaluating the residue gives

$$I_u \simeq -\frac{8\pi^2}{\Delta\Gamma(\Delta)} i^\Delta \left(\frac{p_u}{2} \right)^\Delta \exp \left[-\frac{L^2 u_2^2}{2a^2} \right], \quad (2.67)$$

up to corrections suppressed in the large $p_u a/L$ expansion.

Finally, let us comment on another singularity at $u_1 = u_3$, which comes from the two-point factor $\langle \mathcal{O}_1 \mathcal{O}_3 \rangle$. This singularity is distinct from the observation-point poles $u_1 = u_2$ and $u_3 = u_2$. If one sets $u_1 = u_3$ in the Gaussian part of the shifted integrand, including the prefactor from completing the square, one obtains

$$e^{-\frac{a^2 p_u^2}{2L^2}} \exp \left[-\frac{L^2}{4a^2} \left(u_3 - \frac{ip_u a^2}{L^2} \right)^2 - \frac{L^2}{4a^2} \left(u_3 + \frac{ip_u a^2}{L^2} \right)^2 \right] = \exp \left[-\frac{L^2 u_3^2}{2a^2} \right]. \quad (2.68)$$

Thus this contribution is not exponentially suppressed by $e^{-a^2 p_u^2/(2L^2)}$. Rather, it is subleading because, unlike the contribution obtained by taking residues at both $u_{12} = 0$ and $u_{23} = 0$, it does not receive the same large- $p_u a/L$ enhancement. The leading light-cone peak is therefore produced by the pair of residues at $u_1 = u_2$ and $u_3 = u_2$, while the singularity at $u_1 = u_3$ gives only subleading corrections in the wave-packet regime.

For comparison, the two-point normalization integral in one light-cone sector is

$$J(p) := e^{-\frac{a^2}{2L^2}p^2} \int du_1 du_3 \exp \left[-\frac{L^2}{4a^2} \left(u_1 - \frac{ipa^2}{L^2} \right)^2 - \frac{L^2}{4a^2} \left(u_3 + \frac{ipa^2}{L^2} \right)^2 \right] \frac{1}{(u_{13})^\Delta} \\ \simeq (2\pi)^{3/2} \frac{a}{L} \frac{i^\Delta}{\Gamma(\Delta)} \left(\frac{p}{2} \right)^{\Delta-1}. \quad (2.69)$$

Thus the norm is

$$N_0 \simeq \left(\frac{L}{2} \right)^2 \tilde{C}_{\mathcal{O}J} J(p_u) J(p_v). \quad (2.70)$$

The leading holomorphic numerator from the first term in $F_u(1, 2, 3)$ is

$$N_T^{\text{lead}}(u_2) \simeq \left(\frac{L}{2}\right)^2 \tilde{C}_O \left(-\frac{\Delta}{2L^2}\right) I_u J(p_v). \quad (2.71)$$

Using (2.67) and (2.69), we find the leading contribution to the vacuum-subtracted stress-tensor component,

$$\frac{N_T^{\text{lead}}(u_2)}{N_0} \simeq \frac{\sqrt{2\pi}}{2aL} p_u \exp\left[-\frac{L^2 u_2^2}{2a^2}\right]. \quad (2.72)$$

Because the energy density \mathcal{E} contains an additional factor $1/(2\pi)$, the leading holomorphic contribution is

$$\mathcal{E}_u(t_2, \theta_2) \simeq \frac{1}{2\sqrt{2\pi} aL} p_u \exp\left[-\frac{L^2 u_2^2}{2a^2}\right]. \quad (2.73)$$

The anti-holomorphic contribution is obtained by the exchange

$$u \leftrightarrow v, \quad p_u \leftrightarrow p_v, \quad (2.74)$$

and gives

$$\mathcal{E}_v(t_2, \theta_2) \simeq \frac{1}{2\sqrt{2\pi} aL} p_v \exp\left[-\frac{L^2 v_2^2}{2a^2}\right]. \quad (2.75)$$

Thus the local energy density is

$$\mathcal{E}_{\text{local}}(t_2, \theta_2) \simeq \frac{1}{2\sqrt{2\pi} aL} \left[p_u \exp\left(-\frac{L^2 u_2^2}{2a^2}\right) + p_v \exp\left(-\frac{L^2 v_2^2}{2a^2}\right) \right], \quad (2.76)$$

where

$$u_2 = \frac{t_2 + L\theta_2}{L}, \quad v_2 = \frac{t_2 - L\theta_2}{L}. \quad (2.77)$$

This is the local version of the two null peaks. With the convention above, this local expression carries

$$E_{\text{CFT}}^{\text{phys}} \simeq \frac{p_u + p_v}{2L} = \omega, \quad (2.78)$$

before periodization, as expected from the central frequency of the state. Equivalently, the dimensionless cylinder energy is

$$\Omega_{\text{CFT}} \simeq \frac{p_u + p_v}{2} = \omega L. \quad (2.79)$$

2.7 Periodization on the boundary cylinder

Equation (2.76) gives the contribution from the nearest light-cone poles in the local patch. Near each pole related by the cylinder periodicity, the leading residue calculation is the same after shifting u or v by an integer multiple of 2π . Therefore, in the small-width regime, the

energy density on the cylinder is obtained by summing these leading pole contributions.

Under the angular identification $\theta \sim \theta + 2\pi$, one has

$$u \rightarrow u + 2\pi, \quad v \rightarrow v - 2\pi, \quad (2.80)$$

whereas the single Gaussian factors appearing in (2.76) are not periodic. We therefore define the periodized Gaussian

$$S(x) := \sum_{n \in \mathbb{Z}} \exp \left[-\frac{L^2(x - 2\pi n)^2}{2a^2} \right], \quad S(x + 2\pi) = S(x). \quad (2.81)$$

The periodic energy density is then

$$\mathcal{E}_{\text{cyl}}(t, \theta) \simeq \frac{1}{2\sqrt{2\pi} aL} [p_u S(u) + p_v S(v)]. \quad (2.82)$$

This expression is invariant under $\theta \rightarrow \theta + 2\pi$ and describes two Gaussian peaks propagating along the boundary light-cone directions

$$u = 2\pi n, \quad v = 2\pi n, \quad n \in \mathbb{Z}. \quad (2.83)$$

The locations of the null peaks are independent of the bulk impact parameter. Instead, the impact parameter is encoded in the relative weights of the two chiral components:

$$\frac{p_v - p_u}{p_v + p_u} = \frac{m_0}{\omega L} = b. \quad (2.84)$$

This periodic form is the leading small-width expression associated with the light-cone pole structure of the exact cylinder correlators.

A typical example of the periodic energy density (2.82) is shown in Fig. 2.

3 LCD state and radial null propagation

We now give a second comparison between bulk propagation and boundary energy density. In contrast to the wave-packet state of the previous section, the state considered here is constructed from a local scalar primary operator of large conformal dimension with a Euclidean time regulator. This is the LCD state. The boundary stress tensor can be computed exactly, and the resulting energy density consists of two chiral pulses moving along the boundary light-cone directions. We compare this boundary behavior with the bulk profile.

We consider the state

$$|\Psi_\epsilon\rangle = \mathcal{N} e^{-\epsilon H} \mathcal{O}_\Delta(0)|0\rangle. \quad (3.1)$$

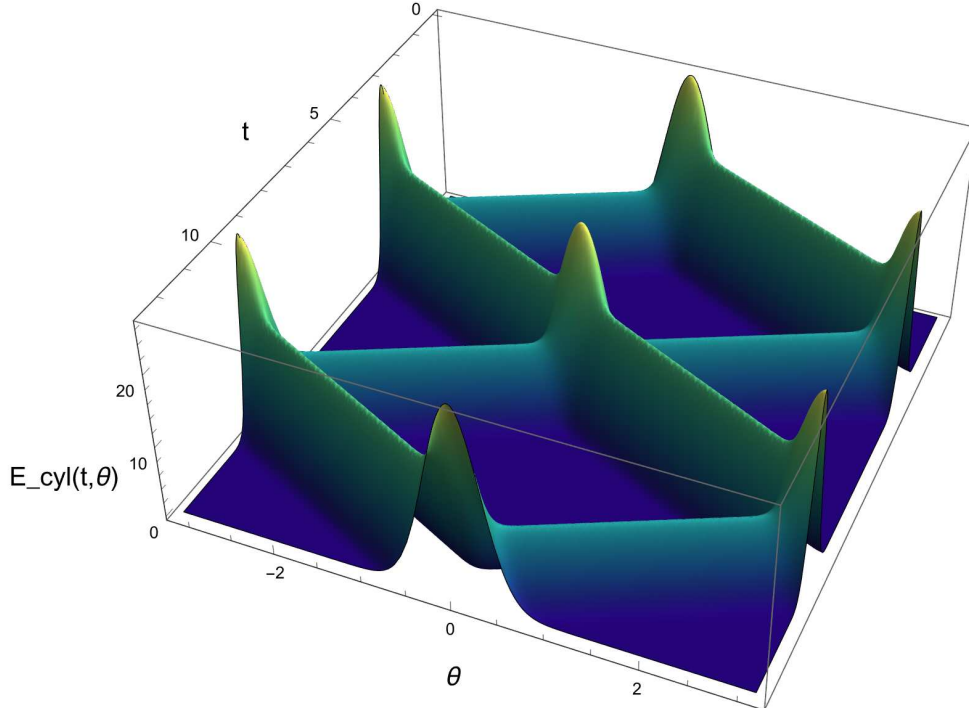


Figure 2: Three-dimensional plot of the periodic energy density (2.82) for $L = 1$, $a = 0.3$, $\omega = 20$, $m_0 = 5$, with the periodic sum truncated at $n_{\max} = 10$, over the ranges $0 \leq t \leq 4\pi L$ and $-\pi \leq \theta \leq \pi$. The two null peaks propagate along $u = \text{const.}$ and $v = \text{const.}$, and reappear periodically as required by the angular periodicity of the cylinder; this is consistent with the pole lattice of the exact cylinder correlators.

Here H denotes the dimensionless cylinder Hamiltonian generating translations in the unit-cylinder time τ . Equivalently, if H_{phys} is the physical Hamiltonian, then $H = LH_{\text{phys}}$, and the physical Euclidean time regulator is $L\epsilon$. This construction is related to earlier studies of holographic local quenches and local-operator excited states, where local CFT excitations were analyzed together with their holographic descriptions [15, 16]. The particular use of primary insertions of large conformal dimension with Euclidean time regulators as localized states in global AdS was developed in [17]. More generally, Euclidean sources provide a way to prepare Lorentzian semiclassical bulk states in holographic CFTs [18].

For large Δ , this state creates a localized semiclassical bulk excitation in the probe regime. We take

$$1 \ll \Delta \ll c, \quad (3.2)$$

so that the dual bulk excitation admits a particle-like semiclassical interpretation while its backreaction can be neglected.³ The Euclidean time regulator ϵ controls the UV energy of the

³More precisely, in the UV-regulated state the typical dimensionless energy is of order $\omega_{\text{typ}} \sim \Delta/\epsilon$. Thus the probe approximation requires $\omega_{\text{typ}} \ll c$, or equivalently $\Delta/\epsilon \ll c$, rather than only $\Delta \ll c$. We will return to this point in Appendix B.

state. In the regime $\epsilon \ll 1$, the typical injected energy is much larger than the rest energy of the dual bulk excitation, and the leading bulk propagation is therefore governed by the null limit of radial propagation. The key question is how this radial null behavior is reflected in the boundary stress tensor.

For the CFT computation in this section, it is convenient to use the unit-cylinder Euclidean coordinate

$$\zeta = \tau_E + i\theta, \quad \bar{\zeta} = \tau_E - i\theta. \quad (3.3)$$

The expectation value of a local operator $X(\zeta, \bar{\zeta})$ is

$$\langle X(\zeta, \bar{\zeta}) \rangle_{\Psi_\epsilon} = \frac{\langle \mathcal{O}^\dagger(\zeta_1, \bar{\zeta}_1) X(\zeta, \bar{\zeta}) \mathcal{O}(\zeta_2, \bar{\zeta}_2) \rangle_{\text{cyl}}}{\langle \mathcal{O}^\dagger(\zeta_1, \bar{\zeta}_1) \mathcal{O}(\zeta_2, \bar{\zeta}_2) \rangle_{\text{cyl}}}, \quad (3.4)$$

with

$$\zeta_1 = +\epsilon, \quad \zeta_2 = -\epsilon. \quad (3.5)$$

Here the ket insertion is at Euclidean time $-\epsilon$, while the bra insertion is at $+\epsilon$.

3.1 Exact cylinder stress tensor

Using the plane-to-cylinder map $z = e^\zeta$, one has

$$z_1 = e^{+\epsilon}, \quad z_2 = e^{-\epsilon}. \quad (3.6)$$

The plane Ward identity gives

$$\frac{\langle T(z) \mathcal{O}(z_1, \bar{z}_1) \mathcal{O}(z_2, \bar{z}_2) \rangle}{\langle \mathcal{O}(z_1, \bar{z}_1) \mathcal{O}(z_2, \bar{z}_2) \rangle} = h \frac{(z_1 - z_2)^2}{(z - z_1)^2 (z - z_2)^2}. \quad (3.7)$$

The cylinder stress tensor is

$$T_{\text{cyl}}(\zeta) = z^2 T_{\text{plane}}(z) - \frac{c}{24}, \quad (3.8)$$

and therefore

$$\langle T(\zeta) \rangle_{\Psi_\epsilon} = \frac{h \sinh^2 \epsilon}{4 \sinh^2 \frac{\zeta + \epsilon}{2} \sinh^2 \frac{\zeta - \epsilon}{2}} - \frac{c}{24}. \quad (3.9)$$

Similarly,

$$\langle \bar{T}(\bar{\zeta}) \rangle_{\Psi_\epsilon} = \frac{h \sinh^2 \epsilon}{4 \sinh^2 \frac{\bar{\zeta} + \epsilon}{2} \sinh^2 \frac{\bar{\zeta} - \epsilon}{2}} - \frac{c}{24}. \quad (3.10)$$

Subtracting the cylinder vacuum contribution,

$$\langle T \rangle_0 = \langle \bar{T} \rangle_0 = -\frac{c}{24}, \quad (3.11)$$

we obtain

$$\delta\langle T(\zeta)\rangle = \frac{h \sinh^2 \epsilon}{4 \sinh^2 \frac{\zeta+\epsilon}{2} \sinh^2 \frac{\zeta-\epsilon}{2}}, \quad \delta\langle \bar{T}(\bar{\zeta})\rangle = \frac{h \sinh^2 \epsilon}{4 \sinh^2 \frac{\bar{\zeta}+\epsilon}{2} \sinh^2 \frac{\bar{\zeta}-\epsilon}{2}}. \quad (3.12)$$

3.2 Lorentzian energy density and comparison with the bulk profile

After Lorentzian continuation

$$\zeta \rightarrow i(\tau + \theta), \quad \bar{\zeta} \rightarrow i(\tau - \theta), \quad (3.13)$$

one finds

$$\delta\langle T(\tau + \theta)\rangle = \frac{h \sinh^2 \epsilon}{4 \left(\sin^2 \frac{\tau+\theta}{2} + \sinh^2 \frac{\epsilon}{2}\right)^2}, \quad \delta\langle \bar{T}(\tau - \theta)\rangle = \frac{h \sinh^2 \epsilon}{4 \left(\sin^2 \frac{\tau-\theta}{2} + \sinh^2 \frac{\epsilon}{2}\right)^2}. \quad (3.14)$$

Hence the vacuum-subtracted stress-tensor component on the unit cylinder is

$$\delta\langle T_{\tau\tau}(\tau, \theta)\rangle = \frac{\Delta \sinh^2 \epsilon}{8} \left[\frac{1}{\left(\sin^2 \frac{\tau+\theta}{2} + \sinh^2 \frac{\epsilon}{2}\right)^2} + \frac{1}{\left(\sin^2 \frac{\tau-\theta}{2} + \sinh^2 \frac{\epsilon}{2}\right)^2} \right]. \quad (3.15)$$

The corresponding energy density is

$$\mathcal{E}_\epsilon^{(\tau)}(\tau, \theta) := \frac{1}{2\pi} \delta\langle T_{\tau\tau}(\tau, \theta)\rangle. \quad (3.16)$$

This exact cylinder result exhibits two chiral pulses moving along the boundary light-cone directions

$$\tau + \theta = 2\pi n, \quad \tau - \theta = 2\pi n, \quad n \in \mathbb{Z}. \quad (3.17)$$

The two pulses meet at the antipodal point after

$$\Delta\tau = \pi \quad (3.18)$$

and return to the original point after one full global period,

$$\Delta\tau = 2\pi. \quad (3.19)$$

This is precisely the sequence of boundary arrivals expected from radial boundary-to-boundary null propagation in global AdS₃.

The dimensionless CFT energy is obtained from the cylinder Hamiltonian as

$$\Omega_{\text{CFT}} = \int_{-\pi}^{\pi} d\theta \mathcal{E}_\epsilon^{(\tau)}(\tau, \theta) = \frac{1}{2\pi} \int_{-\pi}^{\pi} d\theta \delta\langle T_{\tau\tau}(\tau, \theta)\rangle = \Delta \coth \epsilon. \quad (3.20)$$

This exact result gives a useful check on the energy scale of the state. The bulk interpretation, however, is most directly seen from the bulk wave function

$$\Psi_\epsilon(\tau, \rho, \Omega; \Omega_0) = \langle 0 | \Phi(\tau, \rho, \Omega) e^{-\epsilon H} \mathcal{O}_\Delta(0, \Omega_0) | 0 \rangle. \quad (3.21)$$

As shown in Appendix B, this profile has a regulated singularity on the null surface

$$\cos \tau = \sin \rho \Omega \cdot \Omega_0. \quad (3.22)$$

For the radial branch, $\Omega = \Omega_0$, this gives

$$\tau = \frac{\pi}{2} - \rho. \quad (3.23)$$

The same global-mode sum shows that the typical dimensionless energy in the UV-regulated regime is

$$\omega_{\text{typ}} \sim \frac{\Delta}{\epsilon}. \quad (3.24)$$

Restoring the AdS radius, this corresponds to

$$E_{\text{typ}}^{\text{phys}} \sim \frac{\Delta}{L\epsilon}. \quad (3.25)$$

Since the dimensionless rest energy of the dual bulk excitation is $ML \simeq \Delta$, we have

$$\frac{E_{\text{typ}}^{\text{phys}}}{M} = \frac{\omega_{\text{typ}}}{ML} \sim \frac{1}{\epsilon} \gg 1 \quad (3.26)$$

for $\epsilon \ll 1$. Thus the LCD state with the Euclidean time regulator ϵ prepares an ultrarelativistic bulk excitation. The leading bulk propagation is therefore well approximated by the radial null geodesic, namely the $m_0 = 0$ case of the null wave-packet trajectory discussed in Section 2. The exact boundary energy density exhibits the same sequence of boundary arrivals through its two chiral pulses.

4 Discussion

The two examples considered in this paper have different detailed structures, but they convey a common message: the global-cylinder description makes visible a boundary-to-boundary structure that is not manifest in the Poincaré-patch analysis. In global AdS₃, null rays emitted from the boundary reach the antipodal boundary point and return to the original point after one global period. We have shown that this bulk periodicity is reflected in boundary energy densities as periodic chiral structures on the cylinder.

For the wave-packet state, the local residue analysis yields two Gaussian peaks localized

near $u = 0$ and $v = 0$. In the Poincaré-patch analysis these peaks describe the local light-cone propagation of the boundary energy density. On the global cylinder, the exact correlators contain the corresponding lattice of light-cone poles, and the leading small-width result is obtained by summing the local pole contributions near these poles. Thus the two local peaks are promoted to periodic chiral peaks on the cylinder. Their propagation reproduces the arrival at the antipodal boundary point and the return to the original boundary point. The result also makes clear how the bulk impact parameter is encoded in the CFT observable. The locations of the null peaks in the dual CFT are independent of the impact parameter, while the relative weights of the two chiral peaks encode

$$\frac{p_v - p_u}{p_v + p_u} = \frac{m_0}{\omega L} = b.$$

In this sense, the boundary energy density captures part of the conserved data of the bulk null ray, even though it does not literally draw the bulk trajectory.

For the LCD state, the exact cylinder computation gives two periodic pulses moving along the boundary light-cone directions. This provides a second realization of the same global feature: the boundary pulses reach the antipodal point and return to the original point with the same global periodicity as the radial null geodesic described by the regulated bulk profile. The total dimensionless energy is

$$\Omega_{\text{CFT}} = \Delta \coth \epsilon.$$

Since the rest energy of the dual bulk excitation is $ML \simeq \Delta$, the local insertion with $\epsilon \ll 1$ creates an ultrarelativistic excitation,

$$\frac{E_{\text{phys}}}{M} \simeq \frac{1}{\epsilon} \gg 1. \tag{4.1}$$

The leading bulk propagation is therefore well approximated by the radial null geodesic. The important point is that this radial behavior is reflected directly in the exact boundary stress tensor: the two boundary pulses propagate along $\tau \pm \theta = 2\pi n$, reach the antipodal point after $\Delta\tau = \pi$, and return to the original point after $\Delta\tau = 2\pi$. This agrees with the $m_0 = 0$ limit of the wave-packet construction.

Thus, in both examples, the leading bulk propagation relevant for the boundary energy density is described by null geodesics in global AdS. The wave-packet state realizes a general null geodesic with impact parameter $b = m_0/(\omega L)$, whereas the LCD state corresponds to the radial case $b = 0$. The common period 2π and the repeated light-cone pole structure of the cylinder correlators are boundary manifestations of this global-AdS propagation.

Our results are also closely related to the broader idea that bulk causal relations leave characteristic signatures in Lorentzian boundary observables. A basic example is provided by bulk-cone singularities, where Lorentzian CFT correlators become singular when boundary points are connected by bulk null geodesics [8]. Related bulk-cone singularities have also

been studied in black-hole and horizonless AdS geometries [9, 21]. This is also connected to bulk-point singularities and bulk locality in CFT correlators [22–24]. In the present setup, this relation appears in a particularly direct form: the repeated light-cone poles of the exact cylinder correlator produce the periodic boundary energy density, mirroring the boundary-to-boundary propagation and periodicity of null rays in global AdS₃.

There are several natural extensions. One important direction is to study how the global-AdS periodic structure discussed here is modified in black-hole backgrounds. Wave packets in a planar BTZ black hole have already been studied in [25], where it was found that, because of special features of the BTZ geometry and two-dimensional conformal symmetry, the gravitational time delay is not directly visible in the boundary energy density. This suggests that, even in global BTZ, the energy density alone may not be a sufficiently sensitive observable for extracting bulk time delay. Moreover, unlike in global AdS, the global BTZ geometry does not support the same periodic boundary-to-boundary propagation of null rays: the effective potential for null geodesics has no maximum that would turn the ray back toward the boundary, so inward-directed null rays entering from the boundary fall into the black hole [24]. A global-BTZ analysis would therefore clarify how the pure-AdS pole structure and periodic energy density are modified or lost in a black-hole geometry, rather than simply extending the periodic picture found here. The present analysis is restricted to the probe regime. Beyond this regime, gravitational backreaction must be included. A natural approach in the bulk is then to solve the time-dependent bulk Einstein equations and extract the boundary stress tensor from the near-boundary metric using holographic renormalization [26, 27], as in numerical studies of asymptotically AdS collapse and black-hole formation [28]. This would provide a way to study boundary energy densities when the injected energy is large enough to modify the bulk geometry. Another complementary direction is to construct the corresponding high-energy states directly in the CFT. In this respect, it is interesting that bulk wave packets have recently been used to construct CFT states describing black-hole formation and evaporation in AdS/CFT [29]. It would be useful to understand how boundary energy densities behave in such wave-packet states with gravitational backreaction, where the injected energy is large enough to modify the bulk geometry.

Another direction is to understand which aspects of the present result are special to AdS₃/CFT₂. The chiral peak structure found here relies strongly on two-dimensional conformal symmetry and the decomposition into left- and right-moving sectors. In higher-dimensional examples, the boundary energy density associated with a bulk wave packet can be more spatially spread [10]. Comparing the present global-cylinder analysis with higher-dimensional wave packets would help separate universal signatures of bulk propagation from features special to two-dimensional CFTs.

Acknowledgments

The author would like to thank R. Adachi, K. Hashimoto, T. Kawamoto, N. Tanahashi, K. Tasuki and S. Terashima for valuable discussions and helpful comments. The author is particularly grateful to S. Terashima for detailed discussions on the bulk interpretation of the LCD state, which were essential for Appendix B.

During the preparation of this manuscript, the author used ChatGPT (OpenAI) to assist with language editing, organization of the text, and checking the clarity of explanations. The author reviewed and edited all AI-assisted output and takes full responsibility for the content of the manuscript.

A Bulk wave packet from global Klein–Gordon modes

In this appendix, we check the bulk interpretation of the boundary-smeared state used in the main text. We show that the state prepares a bulk one-particle wave packet in the global patch and that, in the high-frequency and small-width regime, its bulk profile is localized around a null geodesic in global AdS₃.

A.1 Global modes and the wave-packet state

We consider a scalar field Φ of mass M in global AdS₃,

$$ds^2 = \frac{L^2}{\cos^2 \rho} (-d\tau^2 + d\rho^2 + \sin^2 \rho d\theta^2), \quad 0 \leq \rho < \frac{\pi}{2}, \quad \theta \sim \theta + 2\pi. \quad (\text{A.1})$$

Here τ is the dimensionless global time, and the corresponding dimensionful boundary time is $t = L\tau$.

The normalizable global modes of a scalar field are standard; see, for example, [30]. We write them as

$$u_{n,m}(\tau, \rho, \theta) = \mathcal{N}_{n,m} e^{-i\Omega_{n,m}\tau + im\theta} R_{n,m}(\rho), \quad (\text{A.2})$$

where

$$R_{n,m}(\rho) = (\cos \rho)^\Delta (\sin \rho)^{|m|} P_n^{(|m|, \Delta-1)}(\cos 2\rho), \quad (\text{A.3})$$

and

$$\Omega_{n,m} = \Delta + |m| + 2n, \quad n = 0, 1, 2, \dots, \quad m \in \mathbb{Z}. \quad (\text{A.4})$$

Here $P_n^{(\alpha, \beta)}$ denotes a Jacobi polynomial, and we use the standard quantization

$$\Delta = 1 + \sqrt{1 + M^2 L^2}. \quad (\text{A.5})$$

The quantized bulk field is expanded as

$$\Phi(\tau, \rho, \theta) = \sum_{n=0}^{\infty} \sum_{m \in \mathbb{Z}} (a_{n,m} u_{n,m}(\tau, \rho, \theta) + a_{n,m}^{\dagger} u_{n,m}^*(\tau, \rho, \theta)). \quad (\text{A.6})$$

We now consider the boundary wave-packet state used in the main text,

$$|\Omega_0, m_0\rangle = \int_{-\infty}^{\infty} d\tau \int_{-\pi}^{\pi} d\theta f_{\Omega_0, m_0}(\tau, \theta) \mathcal{O}(\tau, \theta) |0\rangle, \quad (\text{A.7})$$

with

$$f_{\Omega_0, m_0}(\tau, \theta) = \exp \left[-\frac{\tau^2 + 4 \tan^2(\theta/2)}{2\alpha^2} - i\Omega_0\tau + im_0\theta \right], \quad \alpha = \frac{a}{L}. \quad (\text{A.8})$$

Here $\Omega_0 = \omega L$ is the dimensionless central frequency and m_0 is the central angular momentum. The extrapolate dictionary then relates the boundary primary to the near-boundary limit of the bulk field [5, 30, 31],

$$\mathcal{O}(\tau, \theta) \sim \lim_{\rho \rightarrow \pi/2} (\cos \rho)^{-\Delta} \Phi(\tau, \rho, \theta). \quad (\text{A.9})$$

Therefore the action of the boundary operator on the vacuum can be written as

$$\mathcal{O}(\tau, \theta) |0\rangle = \sum_{n,m} B_{n,m} e^{i\Omega_{n,m}\tau - im\theta} a_{n,m}^{\dagger} |0\rangle. \quad (\text{A.10})$$

We choose the phase convention of the modes so that $B_{n,m}$ is a slowly varying envelope in the large quantum-number regime. Any residual rapidly varying phase in $B_{n,m}$ can equivalently be absorbed into the eikonal action used below, and does not affect the stationary-phase trajectory.

Substituting (A.10) into the smeared state, we obtain a bulk one-particle state

$$|\Omega_0, m_0\rangle = \sum_{n,m} c_{n,m} a_{n,m}^{\dagger} |0\rangle, \quad (\text{A.11})$$

where

$$c_{n,m} \propto B_{n,m} \int d\tau d\theta f_{\Omega_0, m_0}(\tau, \theta) e^{i\Omega_{n,m}\tau - im\theta}. \quad (\text{A.12})$$

For $\alpha \ll 1$, the smearing is localized near $\theta = 0$, so that $2 \tan(\theta/2) \simeq \theta$, and the angular integral over the fundamental domain can be extended to the real line in the Gaussian approximation. We then find

$$c_{n,m} \propto B_{n,m} \exp \left[-\frac{\alpha^2}{2} (\Omega_{n,m} - \Omega_0)^2 - \frac{\alpha^2}{2} (m - m_0)^2 \right]. \quad (\text{A.13})$$

Thus the CFT state prepared by the smearing is, in the bulk one-particle Hilbert space, a

superposition of global modes sharply peaked around

$$\Omega_{n,m} \simeq \Omega_0, \quad m \simeq m_0. \quad (\text{A.14})$$

A.2 Bulk profile and stationary phase

To see how this state propagates in the bulk, we consider the time-dependent bulk profile

$$\Psi_{\text{wp}}(T, \rho, \theta) \equiv \langle 0 | \Phi(T, \rho, \theta) | \Omega_0, m_0 \rangle = \langle 0 | \Phi(0, \rho, \theta) e^{-iHT} | \Omega_0, m_0 \rangle, \quad (\text{A.15})$$

where T is the elapsed dimensionless global time.⁴ Using the mode expansion,

$$\Psi_{\text{wp}}(T, \rho, \theta) = \sum_{n,m} c_{n,m} \mathcal{N}_{n,m} R_{n,m}(\rho) e^{-i\Omega_{n,m}T + im\theta}. \quad (\text{A.16})$$

We evaluate this expression in the high-frequency wave-packet regime

$$\alpha \ll 1, \quad \Omega_0 \gg \Delta, \quad \alpha(\Omega_0 - m_0) \gg 1, \quad \alpha(\Omega_0 + m_0) \gg 1, \quad \Omega_0 > |m_0|. \quad (\text{A.17})$$

The condition $\alpha \ll 1$ means that the wave packet is localized on a scale much smaller than the AdS radius. The inequalities $\alpha(\Omega_0 - m_0) \gg 1$ and $\alpha(\Omega_0 + m_0) \gg 1$ ensure that the smearing contains many oscillations in both light-cone directions. The resulting bulk wave packet therefore has a well-defined central energy Ω_0 and angular momentum m_0 , with the direction of angular motion fixed by the sign of m_0 . The last condition, $\Omega_0 > |m_0|$, ensures that the central ray has a classically allowed radial region, with a turning point satisfying $\sin \rho_* = |m_0|/\Omega_0$.

We now determine the leading phase of the radial wave function. This phase is fixed by the leading eikonal limit of the Klein–Gordon equation. Writing the rapidly varying part of a mode as

$$\exp[iI(T, \rho, \theta)], \quad I(T, \rho, \theta) = -\Omega T + m(\theta - \theta_0) + W(\rho), \quad (\text{A.18})$$

where θ_0 denotes the angular position of the emitted ray. For the state centered at $\theta = 0$ in the main text, one should set $\theta_0 = 0$. The leading Hamilton–Jacobi equation in global AdS₃ is

$$-\Omega^2 + (\partial_\rho W)^2 + \frac{m^2}{\sin^2 \rho} + \frac{M^2 L^2}{\cos^2 \rho} = 0. \quad (\text{A.19})$$

In the regime $\Omega_0 \gg \Delta$, the mass term gives subleading corrections to the central high-frequency ray in the bulk interior. It remains important for the near-boundary falloff of the exact normalizable mode, but it does not affect the leading null trajectory of the wave packet.

⁴This quantity is the analogue of a one-particle wave function in QFT: it is obtained by taking the overlap of the state with the bulk field operator at a spacetime point. See, for example, [32] for a related use of such wave-function.

Thus, for the purpose of determining the central ray, we use the leading null eikonal equation

$$-\Omega^2 + (\partial_\rho W)^2 + \frac{m^2}{\sin^2 \rho} = 0. \quad (\text{A.20})$$

This gives

$$\partial_\rho W = \pm p_\rho(\rho; \Omega, m), \quad p_\rho(\rho; \Omega, m) = \sqrt{\Omega^2 - \frac{m^2}{\sin^2 \rho}}. \quad (\text{A.21})$$

The sign in (A.21) labels the two WKB branches. The branch describing a future-directed ray entering the bulk from the boundary at $T = 0$ has negative radial momentum. We therefore choose the incoming Hamilton–Jacobi action

$$S_{\text{in}}(\rho; \Omega, m) = \int_\rho^{\pi/2} d\rho' \sqrt{\Omega^2 - \frac{m^2}{\sin^2 \rho'}}. \quad (\text{A.22})$$

Indeed,

$$\partial_\rho S_{\text{in}}(\rho; \Omega, m) = -\sqrt{\Omega^2 - \frac{m^2}{\sin^2 \rho}}, \quad (\text{A.23})$$

so this branch has negative radial momentum and hence moves from the boundary toward smaller ρ . In the WKB approximation the corresponding branch of the radial wave function is

$$R_{n,m}^{\text{in}}(\rho) \sim A_{\text{WKB}}(\rho; \Omega, m) \exp[iS_{\text{in}}(\rho; \Omega, m)]. \quad (\text{A.24})$$

We combine the WKB amplitude, the mode normalization, and the slowly varying part of the smearing coefficient into a single smooth prefactor $B_{\text{in}}(\rho; \Omega, m)$. This prefactor affects the overall amplitude of the wave packet at leading order, while the center of the packet is determined by the rapidly varying phase.

Keeping this incoming WKB branch, the bulk profile is locally

$$\begin{aligned} \Psi_{\text{wp}}^{\text{in}} \sim & \int d\Omega dm \exp \left[-\frac{\alpha^2}{2}(\Omega - \Omega_0)^2 - \frac{\alpha^2}{2}(m - m_0)^2 \right] B_{\text{in}}(\rho; \Omega, m) \\ & \times \exp[-i\Omega T + im(\theta - \theta_0) + iS_{\text{in}}(\rho; \Omega, m)]. \end{aligned} \quad (\text{A.25})$$

Here the discrete sum over (n, m) has been approximated by a local integral over (Ω, m) . This is justified in the large quantum-number regime because the wave packet contains many modes within its frequency and angular-momentum widths.

Let

$$\delta\Omega = \Omega - \Omega_0, \quad \delta m = m - m_0. \quad (\text{A.26})$$

Expanding the phase around (Ω_0, m_0) ,

$$S_{\text{in}}(\rho; \Omega, m) = S_{\text{in},0} + \delta\Omega \partial_\Omega S_{\text{in},0} + \delta m \partial_m S_{\text{in},0} + \cdots, \quad (\text{A.27})$$

where

$$S_{\text{in},0} := S_{\text{in}}(\rho; \Omega_0, m_0), \quad B_{\text{in},0} := B_{\text{in}}(\rho; \Omega_0, m_0), \quad (\text{A.28})$$

we obtain

$$\begin{aligned} \Psi_{\text{wp}}^{\text{in}} \sim B_{\text{in},0} e^{i\Theta_0} \int d\delta\Omega d\delta m \exp \left[-\frac{\alpha^2}{2} (\delta\Omega^2 + \delta m^2) + i\delta\Omega (-T + \partial_\Omega S_{\text{in},0}) \right. \\ \left. + i\delta m (\theta - \theta_0 + \partial_m S_{\text{in},0}) \right], \end{aligned} \quad (\text{A.29})$$

with

$$\Theta_0 = -\Omega_0 T + m_0 (\theta - \theta_0) + S_{\text{in},0}. \quad (\text{A.30})$$

Performing the Gaussian integral gives

$$\Psi_{\text{wp}}^{\text{in}} \sim B_{\text{in},0} e^{i\Theta_0} \exp \left[-\frac{(T - \partial_\Omega S_{\text{in},0})^2 + (\theta - \theta_0 + \partial_m S_{\text{in},0})^2}{2\alpha^2} \right]. \quad (\text{A.31})$$

Thus this incoming branch is exponentially supported on

$$T = \partial_\Omega S_{\text{in},0}, \quad \theta - \theta_0 = -\partial_m S_{\text{in},0}. \quad (\text{A.32})$$

These are precisely the Hamilton–Jacobi relations for the null ray generated by S_{in} .

A.3 Null geodesic from the stationary-phase conditions

The stationary-phase conditions above are precisely the Hamilton–Jacobi relations for the incoming branch of a null ray. Defining

$$b = \frac{m_0}{\Omega_0}, \quad (\text{A.33})$$

we have

$$p_\rho(\rho; \Omega_0, m_0) = \Omega_0 \sqrt{1 - \frac{b^2}{\sin^2 \rho}}. \quad (\text{A.34})$$

The derivatives of the incoming Hamilton–Jacobi action give

$$\partial_\Omega S_{\text{in},0} = \int_\rho^{\pi/2} d\rho' \frac{1}{\sqrt{1 - \frac{b^2}{\sin^2 \rho'}}}, \quad (\text{A.35})$$

and

$$\partial_m S_{\text{in},0} = - \int_{\rho}^{\pi/2} d\rho' \frac{b}{\sin^2 \rho' \sqrt{1 - \frac{b^2}{\sin^2 \rho'}}}. \quad (\text{A.36})$$

These derivatives have the standard Hamilton–Jacobi interpretation. The condition

$$T = \partial_{\Omega} S_{\text{in},0} \quad (\text{A.37})$$

gives the elapsed global time from the boundary to the radial position ρ , while

$$\theta - \theta_0 = -\partial_m S_{\text{in},0} \quad (\text{A.38})$$

gives the angular displacement of the center of the wave packet. The minus sign in the second relation follows from our phase convention $\exp[im(\theta - \theta_0)]$ in (A.25).

Let us also derive the corresponding differential form of the trajectory. The incoming Hamilton–Jacobi action is

$$S_{\text{in}}(\rho; \Omega, m) = \int_{\rho}^{\pi/2} d\rho' \sqrt{\Omega^2 - \frac{m^2}{\sin^2 \rho'}}. \quad (\text{A.39})$$

Therefore the radial momentum of the incoming branch is

$$p_{\rho} = \partial_{\rho} S_{\text{in}} = -\sqrt{\Omega^2 - \frac{m^2}{\sin^2 \rho}}. \quad (\text{A.40})$$

The negative sign is the statement that the ray is moving inward, from the boundary toward smaller ρ . The leading eikonal equation is the null Hamilton–Jacobi equation

$$-\Omega^2 + p_{\rho}^2 + \frac{m^2}{\sin^2 \rho} = 0. \quad (\text{A.41})$$

This is the Hamiltonian constraint for a null geodesic in the conformal metric

$$-dT^2 + d\rho^2 + \sin^2 \rho d\theta^2.$$

The conserved quantities are

$$\Omega = -p_T, \quad m = p_{\theta}. \quad (\text{A.42})$$

Using the global time T as the parameter along the ray, the Hamilton equations give

$$\frac{d\rho}{dT} = \frac{p_{\rho}}{\Omega}, \quad \frac{d\theta}{dT} = \frac{m}{\Omega \sin^2 \rho}. \quad (\text{A.43})$$

Defining

$$b = \frac{m}{\Omega}, \quad (\text{A.44})$$

we therefore obtain

$$\left(\frac{d\rho}{dT}\right)^2 = 1 - \frac{b^2}{\sin^2 \rho}, \quad \frac{d\theta}{dT} = \frac{b}{\sin^2 \rho}. \quad (\text{A.45})$$

For the incoming branch one takes the negative sign of $d\rho/dT$. The turning point is determined by

$$\frac{d\rho}{dT} = 0, \quad (\text{A.46})$$

and hence

$$\sin \rho_* = |b|. \quad (\text{A.47})$$

Thus the ratio of the central angular momentum and energy of the packet fixes the radial depth of the null trajectory in the bulk.

For a wave packet emitted from the boundary at $T = 0$ and $\theta = \theta_0$, a convenient parametrization of the corresponding null geodesic is

$$\cos \rho(T) = \sqrt{1 - b^2} \sin T, \quad 0 \leq T \leq \pi, \quad (\text{A.48})$$

and, for $b > 0$,

$$\theta(T) = \theta_0 + \begin{cases} \arctan(b \tan T), & 0 \leq T \leq \pi/2, \\ \pi + \arctan(b \tan T), & \pi/2 \leq T \leq \pi. \end{cases} \quad (\text{A.49})$$

For $b < 0$, the angular displacement has the opposite orientation, but the endpoint is the same antipodal point modulo 2π . Hence the packet reaches the turning point at $T = \pi/2$, arrives at the antipodal boundary point at $T = \pi$, and returns to the original boundary point after one global period, $T = 2\pi$. In terms of the dimensionful boundary time $t = LT$,

$$\Delta t_{\text{bulk}}^{\text{null}} = \pi L, \quad T_{\text{period}} = 2\pi, \quad t_{\text{period}} = 2\pi L. \quad (\text{A.50})$$

Finally, in terms of the boundary parameters used in the main text,

$$\Omega_0 = \omega L, \quad b = \frac{m_0}{\Omega_0} = \frac{m_0}{\omega L}. \quad (\text{A.51})$$

Thus the regime

$$a \ll L, \quad \frac{(\omega L - m_0)a}{L} \gg 1, \quad \frac{(\omega L + m_0)a}{L} \gg 1, \quad \omega L > |m_0| \quad (\text{A.52})$$

is the regime in which the boundary-smeared state creates a localized bulk wave packet following a null geodesic in global AdS_3 .

B Bulk interpretation of the LCD state

In this appendix we examine the bulk interpretation of the state constructed from a local scalar primary insertion of large conformal dimension with a Euclidean time regulator. We refer to it as the LCD state. We work in the probe regime. The operator dimension is taken to satisfy $1 \ll \Delta$, so that the dual bulk excitation admits a semiclassical particle interpretation, but its backreaction is neglected. Since the global frequencies used below are dimensionless, we use the dimensionless global time τ in this appendix. The Hamiltonian H in $e^{-\epsilon H}$ is the corresponding dimensionless cylinder Hamiltonian, and ϵ is a dimensionless Euclidean time regulator. Equivalently, if H_{phys} is the physical Hamiltonian, then $H = LH_{\text{phys}}$, and the physical Euclidean time regulator is $L\epsilon$.

Using global AdS normal modes, we compute the regulated bulk profile

$$\Psi_\epsilon(\tau, \rho, \hat{n}; \hat{n}_0) := \langle 0 | \Phi(\tau, \rho, \hat{n}) e^{-\epsilon H} \mathcal{O}_\Delta(0, \hat{n}_0) | 0 \rangle. \quad (\text{B.1})$$

This quantity is an unnormalized bulk wave function associated with the LCD state. The overall normalization will not affect the location of the leading singular support or the estimate of the typical energy scale. Here \hat{n} and \hat{n}_0 denote angular positions on S^{d-1} .

We use the global AdS mode expansion

$$\Phi(\tau, \rho, \hat{n}) = \sum_{n,l,m} \psi_{nl}(\rho) \left[a_{nlm} e^{-i\omega_{nl}\tau} Y_{lm}^*(\hat{n}) + a_{nlm}^\dagger e^{i\omega_{nl}\tau} Y_{lm}(\hat{n}) \right], \quad (\text{B.2})$$

where

$$\omega_{nl} = 2n + l + \Delta \quad (\text{B.3})$$

is the dimensionless global energy, and

$$\psi_{nl}(\rho) = \frac{1}{\mathcal{N}_{nl}} \sin^l \rho \cos^\Delta \rho P_n^{l+d/2-1, \Delta-d/2}(\cos 2\rho). \quad (\text{B.4})$$

The corresponding CFT primary on the cylinder is expanded in the same creation and annihilation operators as

$$\mathcal{O}_\Delta(\tau, \hat{n}) = \sum_{n,l,m} \psi_{nl}^{\text{CFT}} \left[Y_{lm}(\hat{n}) e^{i\omega_{nl}\tau} a_{nlm}^\dagger + Y_{lm}^*(\hat{n}) e^{-i\omega_{nl}\tau} a_{nlm} \right], \quad (\text{B.5})$$

with

$$\psi_{nl}^{\text{CFT}} = \left[\frac{2}{\pi} \frac{\Gamma(d/2)}{\Gamma(\Delta)\Gamma(\Delta+1-d/2)} \right]^{1/2} \left[\frac{\Gamma(n+\Delta+1-d/2)\Gamma(n+l+\Delta)}{\Gamma(n+1)\Gamma(n+l+d/2)} \right]^{1/2}. \quad (\text{B.6})$$

These formulae follow from applying the extrapolate dictionary to global AdS normal modes

[5, 30, 31].

Acting on the vacuum, the boundary operator creates the one-particle state

$$\mathcal{O}_\Delta(0, \hat{n}_0)|0\rangle = \sum_{n,l,m} \psi_{nl}^{\text{CFT}} Y_{lm}(\hat{n}_0) a_{nlm}^\dagger |0\rangle. \quad (\text{B.7})$$

The Euclidean time regulator gives

$$e^{-\epsilon H} a_{nlm}^\dagger |0\rangle = e^{-\epsilon \omega_{nl}} a_{nlm}^\dagger |0\rangle. \quad (\text{B.8})$$

Only the annihilation part of the bulk field contributes in (B.1). Therefore

$$\Psi_\epsilon(\tau, \rho, \hat{n}; \hat{n}_0) = \sum_{n,l,m} \psi_{nl}(\rho) \psi_{nl}^{\text{CFT}} e^{-(\epsilon+i\tau)\omega_{nl}} Y_{lm}^*(\hat{n}) Y_{lm}(\hat{n}_0). \quad (\text{B.9})$$

This is the regulated bulk wave function written entirely in global modes.

This mode sum is the global bulk-to-boundary Wightman function with the boundary time shifted by $-i\epsilon$. Up to an overall normalization convention,

$$\Psi_\epsilon(\tau, \rho, \hat{n}; \hat{n}_0) = \mathcal{C}_\Delta \left[\frac{\cos \rho}{2 \{ \cos(\tau - i\epsilon) - \sin \rho \hat{n} \cdot \hat{n}_0 \}} \right]^\Delta. \quad (\text{B.10})$$

For small ϵ ,

$$\cos(\tau - i\epsilon) = \cos \tau + i\epsilon \sin \tau + O(\epsilon^2). \quad (\text{B.11})$$

Thus the regulated singularity lies on

$$\cos \tau = \sin \rho \hat{n} \cdot \hat{n}_0. \quad (\text{B.12})$$

This is the bulk light cone emanating from the boundary insertion. In the radial direction $\hat{n} = \hat{n}_0$, it gives

$$\cos \tau = \sin \rho, \quad \tau = \frac{\pi}{2} - \rho, \quad (\text{B.13})$$

which is the incoming radial null geodesic.

We now estimate the energy scale from the same mode sum. At the center of AdS, $\rho = 0$, only the $l = 0$ modes contribute because of the factor $\sin^l \rho$ in (B.4). Hence

$$\Psi_\epsilon(\tau, 0) = \sum_{n=0}^{\infty} \psi_{n0}(0) \psi_{n0}^{\text{CFT}} e^{-(\epsilon+i\tau)(2n+\Delta)}. \quad (\text{B.14})$$

The n -dependence of the coefficient can be read off directly from the closed form (B.10).

Setting $z = \tau - i\epsilon$, the profile at $\rho = 0$ is

$$\Psi_\epsilon(\tau, 0) \propto \left(\frac{1}{2 \cos z} \right)^\Delta = e^{-i\Delta z} (1 + e^{-2iz})^{-\Delta}. \quad (\text{B.15})$$

Using

$$(1 + x)^{-\Delta} = \sum_{n=0}^{\infty} (-1)^n \frac{\Gamma(n + \Delta)}{\Gamma(\Delta)\Gamma(n + 1)} x^n, \quad (\text{B.16})$$

we obtain

$$\Psi_\epsilon(\tau, 0) \propto e^{-(\epsilon+i\tau)\Delta} \sum_{n=0}^{\infty} (-1)^n \frac{\Gamma(n + \Delta)}{\Gamma(n + 1)} e^{-2n(\epsilon+i\tau)}. \quad (\text{B.17})$$

Here the n -independent factor $1/\Gamma(\Delta)$ has been absorbed into the overall normalization. For the magnitude of the mode weight,

$$w_n \sim \frac{\Gamma(n + \Delta)}{\Gamma(n + 1)} e^{-2\epsilon n}. \quad (\text{B.18})$$

At large n ,

$$\frac{\Gamma(n + \Delta)}{\Gamma(n + 1)} \sim n^{\Delta-1}. \quad (\text{B.19})$$

Therefore the dominant contribution is determined by the saddle of

$$\log w_n \simeq (\Delta - 1) \log n - 2\epsilon n. \quad (\text{B.20})$$

The saddle condition gives

$$\frac{\Delta - 1}{n} - 2\epsilon = 0, \quad n_{\text{typ}} \simeq \frac{\Delta}{2\epsilon}. \quad (\text{B.21})$$

The corresponding dimensionless global energy is

$$\omega_{\text{typ}} = 2n_{\text{typ}} + \Delta \sim \frac{\Delta}{\epsilon}. \quad (\text{B.22})$$

This estimate was already obtained in [17], and is also consistent with the CFT result (3.20). This is not a dimensionful energy. Restoring the AdS radius,

$$E_{\text{typ}}^{\text{phys}} = \frac{\omega_{\text{typ}}}{L} \sim \frac{\Delta}{L\epsilon}. \quad (\text{B.23})$$

For a scalar field dual to a scalar primary operator of conformal dimension Δ ,

$$M^2 L^2 = \Delta(\Delta - d), \quad ML \simeq \Delta. \quad (\text{B.24})$$

Thus ML is the dimensionless rest energy of the dual bulk excitation, while M is its physical rest energy. Hence

$$\frac{E_{\text{typ}}^{\text{phys}}}{M} = \frac{\omega_{\text{typ}}}{ML} \sim \frac{1}{\epsilon}. \quad (\text{B.25})$$

In the regime $\epsilon \ll 1$, the LCD state describes a highly relativistic bulk excitation. At the same time, the more precise condition for neglecting gravitational backreaction is not simply $\Delta \ll c$, but rather

$$\omega_{\text{typ}} \sim \frac{\Delta}{\epsilon} \ll c. \quad (\text{B.26})$$

This is because the strength of the backreaction is controlled by the dimensionless energy $E_{\text{typ}}^{\text{phys}}L \simeq \omega_{\text{typ}}$. Under this probe-limit condition, the leading bulk propagation is governed by the null limit of the semiclassical excitation.

References

- [1] J. M. Maldacena, “The Large N limit of superconformal field theories and supergravity,” *Adv. Theor. Math. Phys.* **2** (1998) 231–252, [arXiv:hep-th/9711200](#).
- [2] S. S. Gubser, I. R. Klebanov, and A. M. Polyakov, “Gauge theory correlators from noncritical string theory,” *Phys. Lett. B* **428** (1998) 105–114, [arXiv:hep-th/9802109](#).
- [3] E. Witten, “Anti-de Sitter space and holography,” *Adv. Theor. Math. Phys.* **2** (1998) 253–291, [arXiv:hep-th/9802150](#).
- [4] A. Hamilton, D. N. Kabat, G. Lifschytz, and D. A. Lowe, “Local bulk operators in AdS/CFT: A boundary view of horizons and locality,” *Phys. Rev. D* **73** (2006) 086003, [arXiv:hep-th/0506118](#).
- [5] A. Hamilton, D. N. Kabat, G. Lifschytz, and D. A. Lowe, “Holographic representation of local bulk operators,” *Phys. Rev. D* **74** (2006) 066009, [arXiv:hep-th/0606141](#).
- [6] D. Kabat, G. Lifschytz, and D. A. Lowe, “Constructing local bulk observables in interacting AdS/CFT,” *Phys. Rev. D* **83** (2011) 106009, [arXiv:1102.2910 \[hep-th\]](#).
- [7] D. Harlow, “TASI Lectures on the Emergence of Bulk Physics in AdS/CFT,” *PoS TASI2017* (2018) 002, [arXiv:1802.01040 \[hep-th\]](#).
- [8] V. E. Hubeny, H. Liu, and M. Rangamani, “Bulk-cone singularities and signatures of horizon formation in AdS/CFT,” *JHEP* **01** (2007) 009, [arXiv:hep-th/0610041](#).
- [9] M. Dodelson, C. Iossa, R. Karlsson, A. Lupsasca, and A. Zhiboedov, “Black hole bulk-cone singularities,” *JHEP* **07** (2024) 046, [arXiv:2310.15236 \[hep-th\]](#).

- [10] N. Tanahashi, S. Terashima, and S. Yoshikawa, “Holographic description of bulk wave packets in $\text{AdS}_4/\text{CFT}_3$,” *JHEP* **06** (2025) 214, [arXiv:2503.11485 \[hep-th\]](#).
- [11] S. Terashima, “Bulk locality in the AdS/CFT correspondence,” *Phys. Rev. D* **104** no. 8, (2021) 086014, [arXiv:2005.05962 \[hep-th\]](#).
- [12] M. Gary, S. B. Giddings, and J. Penedones, “Local bulk S-matrix elements and CFT singularities,” *Phys. Rev. D* **80** (2009) 085005, [arXiv:0903.4437 \[hep-th\]](#).
- [13] M. Gary and S. B. Giddings, “The Flat space S-matrix from the AdS/CFT correspondence?,” *Phys. Rev. D* **80** (2009) 046008, [arXiv:0904.3544 \[hep-th\]](#).
- [14] S. Terashima, “Wave packets in AdS/CFT correspondence,” *Phys. Rev. D* **109** no. 10, (2024) 106012, [arXiv:2304.08478 \[hep-th\]](#).
- [15] M. Nozaki, T. Numasawa, and T. Takayanagi, “Holographic Local Quenches and Entanglement Density,” *JHEP* **05** (2013) 080, [arXiv:1302.5703 \[hep-th\]](#).
- [16] P. Caputa, M. Nozaki, and T. Takayanagi, “Entanglement of local operators in large- N conformal field theories,” *PTEP* **2014** (2014) 093B06, [arXiv:1405.5946 \[hep-th\]](#).
- [17] D. Berenstein and J. Simon, “Localized states in global AdS space,” *Phys. Rev. D* **101** no. 4, (2020) 046026, [arXiv:1910.10227 \[hep-th\]](#).
- [18] D. Marolf, O. Parrikar, C. Rabideau, A. Izadi Rad, and M. Van Raamsdonk, “From Euclidean Sources to Lorentzian Spacetimes in Holographic Conformal Field Theories,” *JHEP* **06** (2018) 077, [arXiv:1709.10101 \[hep-th\]](#).
- [19] Y. Jia and M. Kulaxizi, “Bulk Phase Shift and Singularity,” [arXiv:2602.06558 \[hep-th\]](#).
- [20] D. Simmons-Duffin, “Tasi lectures on conformal field theory in lorentzian signature,” https://www.desy.de/~bargheer/string-journal-club/presentations/2023-05-16_Sebastian-Harris_Simmons-Duffin:_TASI-Lorentzian-CFT.pdf.
- [21] H.-Y. Chen, Y. Hikida, and Y. Koga, “Bulk-cone singularities and echoes from AdS exotic compact objects,” *JHEP* **04** (2026) 210, [arXiv:2512.21535 \[hep-th\]](#).
- [22] R. Bousso, B. Freivogel, S. Leichenauer, V. Rosenhaus, and C. Zukowski, “Null Geodesics, Local CFT Operators and AdS/CFT for Subregions,” *Phys. Rev. D* **88** (2013) 064057, [arXiv:1209.4641 \[hep-th\]](#).
- [23] J. Maldacena, D. Simmons-Duffin, and A. Zhiboedov, “Looking for a bulk point,” *JHEP* **01** (2017) 013, [arXiv:1509.03612 \[hep-th\]](#).

- [24] S. Kinoshita, K. Murata, and D. Takeda, “Shooting null geodesics into holographic spacetimes,” *JHEP* **10** (2023) 074, [arXiv:2304.01936 \[hep-th\]](#).
- [25] N. Tanahashi, S. Terashima, and S. Yoshikawa, “Probing Black Hole Thermal Effects in the Dual CFT via Wave Packets,” [arXiv:2601.04647 \[hep-th\]](#).
- [26] V. Balasubramanian and P. Kraus, “A Stress tensor for Anti-de Sitter gravity,” *Commun. Math. Phys.* **208** (1999) 413–428, [arXiv:hep-th/9902121](#).
- [27] S. de Haro, K. Skenderis, and S. N. Solodukhin, “Holographic reconstruction of space-time and renormalization in the AdS/CFT correspondence,” *Commun. Math. Phys.* **217** (2001) 595–622, [arXiv:hep-th/0002230](#).
- [28] H. Bantilan, F. Pretorius, and S. S. Gubser, “Simulation of Asymptotically AdS5 Spacetimes with a Generalized Harmonic Evolution Scheme,” *Phys. Rev. D* **85** (2012) 084038, [arXiv:1201.2132 \[hep-th\]](#).
- [29] J. de Boer, J. Hollander, and A. Rolph, “A Reverse Black Hole Information Problem,” [arXiv:2601.22077 \[hep-th\]](#).
- [30] V. Balasubramanian, P. Kraus, and A. E. Lawrence, “Bulk versus boundary dynamics in anti-de Sitter space-time,” *Phys. Rev. D* **59** (1999) 046003, [arXiv:hep-th/9805171](#).
- [31] T. Banks, M. R. Douglas, G. T. Horowitz, and E. J. Martinec, “AdS dynamics from conformal field theory,” [arXiv:hep-th/9808016](#).
- [32] S. Shibuya and S. Sugishita, “Notes on Rindler wave packets in Minkowski spacetime,” *Phys. Rev. D* **112** no. 12, (2025) 125007, [arXiv:2505.20078 \[hep-th\]](#).